J. Space Weather Space Clim. 2018, 8, A45

https://doi.org/10.1051/swsc/2018036

JSWSC

Available online at:
www.swsc-journal.org

RESEARCH ARTICLE OPEN ACCESS

Winter anomaly in N_mF_2 and TEC: when and where it can occur

Yury V. Yasyukevich[1], Anna S. Yasyukevich[1,*], Konstantin G. Ratovsky[1], Maxim V. Klimenko[2], Vladimir V. Klimenko[2], and Nikolay V. Chirik[2,3]

[1] Institute of Solar-Terrestrial Physics SB RAS, p/o box 291, 126a Lermontov str., Irkutsk 664033, Russian Federation
[2] West Department of Pushkov IZMIRAN RAS, 41 Pobedy avenue, Kaliningrad 236017, Russian Federation
[3] Immanuel Kant Baltic Federal University, 14 A Nevsky str., Kaliningrad 236041, Russian Federation

Received 6 April 2018 / Accepted 18 September 2018

Abstract – For the first time, by using a regression procedure, we analyzed the solar activity dependence of the winter anomaly intensity in the ionospheric F2-layer peak electron density (N_mF_2) and in the Total Electron Content (TEC) on a global scale. We used the data from global ionospheric maps for 1998–2015, from GPS radio occultation observations with COSMIC, CHAMP, and GRACE satellites for 2001–2015, and ground-based ionosonde data. The fundamental features of the winter anomaly in N_mF_2 and in TEC (spatial distribution and solar activity dependence) are similar for these parameters. We determined the regions, where the winter anomaly may be observed in principle, and the solar activity level, at which the winter anomaly may be recorded in different sectors. A growth in geomagnetic disturbance or in the solar activity level is shown to facilitate the winter anomaly intensity increase. Longitudinal variations in the winter anomaly intensity do not conform partly to the generally accepted Rishbeth theory. We consider the obtained results in the context of spatial and solar cycle variations in O/N_2 ratio and thermospheric meridional wind. Additionally, we briefly discuss different definitions of the winter anomaly.

Keywords: winter anomaly / peak electron density / TEC / ionosphere / solar activity / geomagnetic disturbances / longitudinal variation

1 Introduction

1.1 Historical definition

The term "anomaly" originally meant any deviations from "solar-controlled behaviour" in which the critical frequency f_oF_2 (proportional to the square root of the peak electron density, N_mF_2) varies regularly with the solar zenith angle χ as it does in the well-known Chapman layer (Rishbeth, 1998). In particular, the winter anomaly is a phenomenon consisting in the fact that mid-latitude daytime N_mF_2 (or f_oF_2) is greater in winter than in summer at approximately the same solar activity level (Torr & Torr, 1973; Zou et al., 2000). Burns et al. (2012, 2014) proposed an alternative definition of the winter anomaly as the ratio of the median N_mF_2 in the winter hemisphere to the median N_mF_2 in the summer hemisphere for the same solstice (December or June). We do not undertake to state which definition is more correct, but we will compare features of the winter anomaly for its different definitions in the Discussion part.

*Corresponding author: annpol@iszf.irk.ru

1.2 Empirical studies of the winter anomaly on the global scale

Torr & Torr (1973) using the data of 140 ionosondes in 1958, 1964, and 1969 (high, low and moderate solar activity, respectively) constructed global maps showing the regions where monthly median noon f_oF_2 is greatest in different seasons. From these maps it is seen that the North American sector is the region where f_oF_2 is greatest in winter under any solar activity level. With increasing solar activity, the area of the winter maximum expands and covers, at solar maximum, much of the Northern Hemisphere and the "Australian sector" in the Southern Hemisphere. Here and further in the text as the "Australian sector" we call the domain of the Southern Hemisphere middle latitudes in the range of about 45–135°E.

Pavlov & Pavlova (2012) using the data of 98 ionosondes for 1957–2009 concluded that the occurrence probability of the winter anomaly and the daytime N_mF_2 winter/summer ratio did not decrease with increasing solar activity and correlated much stronger with geomagnetic latitude than with geographic one.

Lee et al. (2011) investigated the height, local time, latitude, longitude, and hemispheric variations of the electron density analyzing the COSMIC satellites data measured in 2007 (low solar activity). The authors concluded that the winter anomaly was stronger in the Northern Hemisphere, and a more intense winter anomaly occurred in the region closer to the magnetic pole.

1.3 Theoretical explanation of the winter anomaly

The explanation of the winter anomaly given by Rishbeth (1998), Zou et al. (2000), and Rishbeth et al. (2000) is based on seasonal neutral composition changes (density ratio of atomic oxygen to molecular nitrogen O/N_2 is greater in winter than in summer). In its turn, these composition changes are due to the global thermospheric circulation with upwelling zone (reduced O/N_2) in the summer hemisphere and downwelling zone (enhanced O/N_2) in the winter hemisphere, just equatorward of the auroral oval. The geographic latitude of winter downwelling zone depends on the geomagnetic longitude. This latitude is lower in "near-the-pole" sectors (American in the Northern Hemisphere and Australian in the Southern Hemisphere) than in "far-from-the-pole" sectors (East-Siberian in the Northern Hemisphere and American in the Southern Hemisphere). The lower latitude (and consequently larger $\cos\chi$) leads to greater increase in N_mF_2 in "near-the-pole" sectors compared to "far-from-the-pole" sectors. The given explanation was successfully reproduced by the CTIP model (Zou et al., 2000). Note, that the CTIP model could not reproduce the enhancement of the winter anomaly with increasing solar activity, as well as stronger winter anomaly in the Northern Hemisphere than in the Southern one. Later proposed were some corrections and additions of this mechanism, including: analysis of the role of vibrationally excited molecules (Torr et al., 1980; Pavlov & Pavlova, 2005), and investigation of Equatorial Ionization Anomaly (EIA) indirect influence on winter anomaly formation (Qian et al., 2016a, 2016b).

Burns et al. (2014) showed that N_mF_2 winter-to-summer ratio is large at the solar maximum and small at the solar minimum. Analyzing the O/N_2 ratio measured by GUVI they concluded that this feature was mainly explained by the greater winter-to-summer differences of O/N_2 in solar maximum than in solar minimum, with a secondary contribution (according to NRL-MSIS model results) from the effects of temperature on the recombination coefficient between O^+ and the molecular neutral gas. According to Qian et al. (2016a), the EIA interrupts the solar heating-induced summer-to-winter meridional wind. This interruption occurs primarily due to plasma-neutral collisional heating, which maximizes near the EIA. This EIA-associated heating counteracts the summer-to-winter pressure gradient in the summer hemisphere but increases the pressure gradients in the winter hemisphere. The summer-to-winter wind is suppressed as it encounters the EIA in the summer hemisphere but accelerates again at mid-latitudes in the winter hemisphere after it passes through the EIA. The meridional wind then converges as equator-pole pressure gradients diminish at high latitudes and is countered by Joule heating in auroral regions, creating an opposing pressure gradient. This convergence and thus downwelling causes large values of O/N_2 at subauroral latitudes in the winter hemisphere. The EIA effect is stronger near the December solstice than near the June one. This December-June difference is attributed to the ionospheric annual asymmetry: electron density is larger near the December solstice than near the June one (Mendillo et al., 2005). As a result, the meridional wind convergence and downwelling at subauroral latitudes in the winter hemisphere are stronger in December than in June.

1.4 Winter anomaly in other ionospheric parameters

The definition of the winter anomaly given initially for N_mF_2 (or f_oF_2) may be applied for other ionospheric parameters. Considering the winter anomaly in the electron density at a given height $N_e(h)$, it was found that the winter anomaly exists only over a limited height range (from ~180 km up to 400–500 km) around the peak height (King et al., 1968; Fatkullin, 1970; Boenkova & Mednikova, 1972; Lee et al., 2011; Mikhailov & Perrone, 2014). The detailed explanation of this feature was given by Mikhailov & Perrone (2014).

The winter anomaly in the Total Electron Content (TEC) was first studied by Zhao et al. (2007). They used the NASA-JPL Global Ionospheric Maps (GIM) from 1999 to 2005 as a source of TEC. The results revealed that the longitudinal dependence as well as the solar activity behavior of the winter anomaly in TEC is close to those in N_mF_2.

Huo et al. (2009), while studying the winter anomaly in TEC during high solar activity (in 2002), revealed that the winter-summer difference in TEC is strongest at North American mid-latitudes and the TEC winter anomaly is stronger in the Russia-Asia region than in Europe. Such a pattern was not completely consistent with the variations in O/N_2 from the NRLMSISE-00 model with the highest values in the East-Siberian regions and the lowest values in North America. The authors assumed that the TEC winter anomaly is stronger in the East-Siberian than at European regions due to corresponding changes in the O/N_2 ratio, whereas in North America the TEC winter anomaly was strongly affected by the both magnetospheric processes and the O/N_2 ratio.

1.5 The purpose of this study

Recent papers that focused on the winter anomaly study (Lee et al., 2011; Pavlov & Pavlova, 2012; Burns et al., 2014; Mikhailov & Perrone, 2014; Lee et al., 2014) demonstrated the importance of this topic in the ionospheric community and some uncertainties that should be resolved. Historically, the winter anomaly was found and studied using N_mF_2 (or f_oF_2) from ionosonde observations, but the global ionosonde distribution is not uniform and does not cover all world regions. At present, there are observed ionospheric parameters having near uniform geographic distribution, e.g. TEC from the GIM or N_mF_2 from the data of Radio Occultation (RO) measurements. At the same time, there is a question about differences in the winter anomaly manifestation in N_mF_2 and TEC. The main purpose of this study is to compare the geographical features (interhemispheric asymmetry and longitudinal variations) and the solar activity dependence of the winter anomaly in N_mF_2 from ionosondes and RO data, and in TEC from the GIM. Additionally, we estimate the solar activity levels at which the winter anomaly in N_mF_2 and in TEC appears in various geographical regions, as well as the geomagnetic activity influence on the winter anomaly in TEC. The key

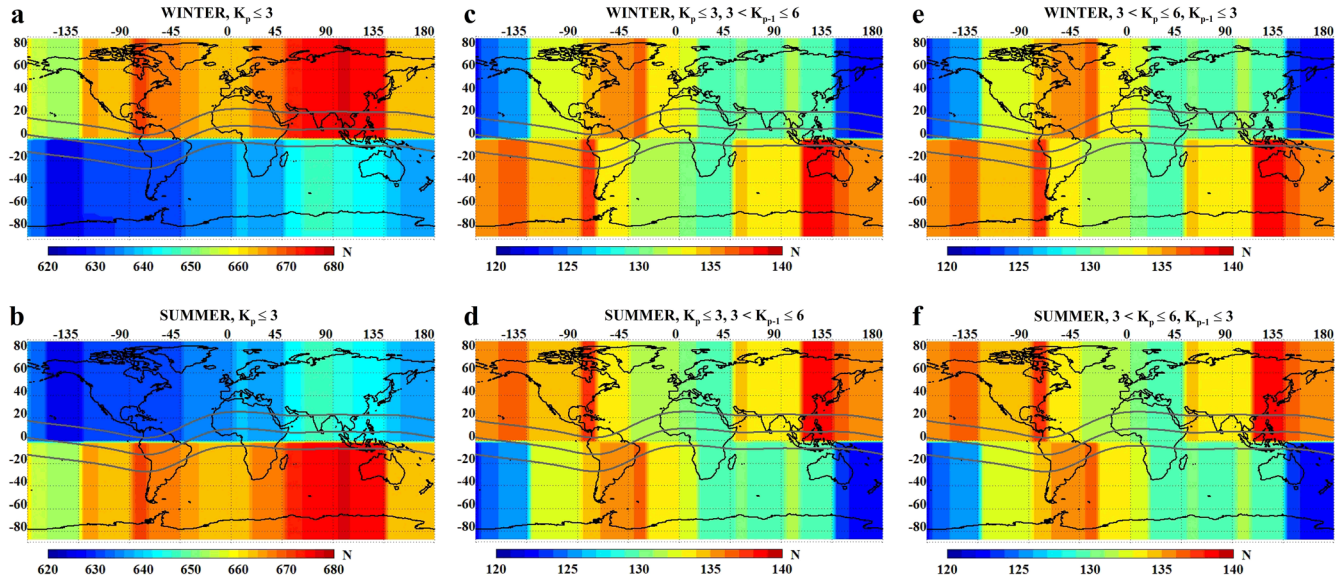

Fig. 1. Number of data points used for TEC winter/summer ratio calculation at different geomagnetic conditions: (a), (b) K_p in the last 24 h did not surpass 3; (c), (d) K_p in the last 24 h did not surpass 3, but in the last 48 h it was recorded $3 < K_{p-1} \le 6$; (e), (f) K_p did not surpass 3 in the last 48 h, except recording $3 < K_p \le 6$ at least once in the last 24 h. Bold gray curves are the geomagnetic equator and ±15° geomagnetic latitudes.

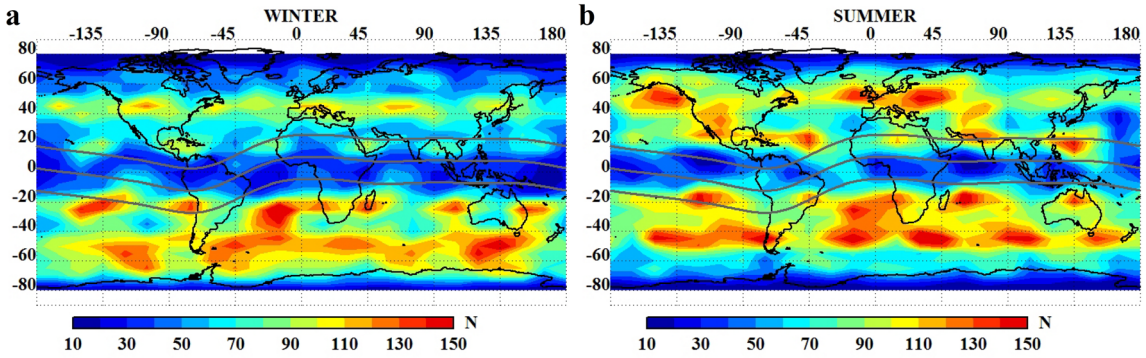

Fig. 2. Number of data points used for N_mF_2 winter/summer ratio calculation. Bold gray curves are the geomagnetic equator and ±15° geomagnetic latitudes.

issue of this study was also to reveal the regions, where the winter anomaly can be observed in principle at different levels of solar and geomagnetic activity. For explanation of the obtained results we analyze spatial and solar cycle variations in thermospheric wind and O/N_2 ratio.

2 Data and their processing

To analyze the winter anomaly in N_mF_2 we used data from RO observations with COSMIC, CHAMP, and GRACE for 2001–2015 as well as ionosonde data published in Pavlov & Pavlova (2012). As ionosonde data, we used average winter anomaly intensity $\langle R \rangle$ (Table 1 in Pavlov & Pavlova, 2012). $\langle R \rangle$ was calculated by Pavlov & Pavlova (2012) through occurrence probability function $P(R)$.

For separating the data according to solar activity level, Pavlov & Pavlova (2012) used the current $F_{10.7}$ value, the $F_{10.7p}$ value for the previous day, and also the $F_{10.7m}$ index which is mean for 81 days with the current day as the center. They presented results for three solar activity levels: low activity (all three parameters were <100 *s.f.u.*), moderate activity (if one of the parameters was within the 100–170 *s.f.u.* range), and high activity (one of the parameters surpassed 170 *s.f.u.*). Hereinafter, *s.f.u.* is solar flux unit (1 *s.f.u.* = 10^{-22} Wm^{-2} Hz^{-1}). In that case, all the days, for which the previous-day K_p surpassed 3 at least once, were excluded from consideration. To analyze the winter anomaly in TEC, we used TEC global ionospheric maps for 1998–2015. GIM involve absolute TEC values for the entire globe with the 2.5° latitude and 5° longitude spatial resolution. The total dynamics of GIM TEC from different laboratories generally agrees, despite systematic differences (Afraimovich et al., 2008). We used the JPL TEC

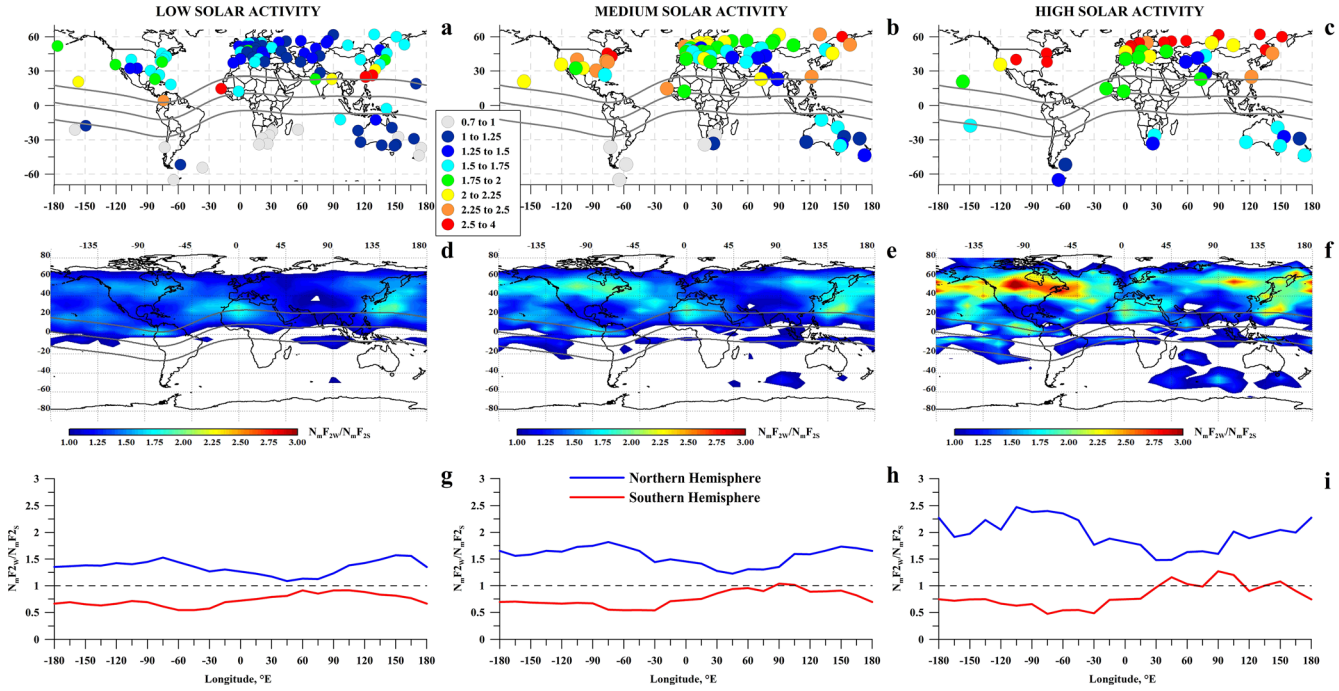

Fig. 3. Maps for the N_mF_2 winter anomaly intensity distribution from Pavlov and Pavlova (2012) (a)–(c) and from the RO measurements (d)–(f), as well as the longitudinal variation of the N_mF_2 winter anomaly intensity averaged at 40–60° geographic latitudinal bands based on the RO data (g)–(i). Panels (a, d, g) correspond to low solar activity; (b), (e), (h) correspond to moderate solar activity; and (c), (f), (i) display high solar activity. White color on panels (d)–(f) shows the regions, for which the winter/summer ratio is less than 1. Bold gray curves (a)–(f) are the geomagnetic equator and ±15° geomagnetic latitudes.

maps (Mannucci et al., 1998; Hernández-Pajares et al., 2009). Estimating the levels of solar and geomagnetic activity was based on the K_p and $F_{10.7}$ indexes (http://www.ngdc.noaa.gov/stp/GEOMAG/kp_ap.html).

As the winter anomaly intensity, we considered the ratio of midday (12–13 LT) TEC and RO N_mF_2 values in the winter period to the midday values in the summer period. For the Northern Hemisphere for summer conditions, we chose the period with center in the June solstice ±30 days. For winter conditions, this period involved the December solstice ±30 days. The choice for the Southern Hemisphere was exactly opposite. At such an approach, there is a disruption in the equatorial region. One should note, however, that the winter anomaly is, by definition, a mid-latitude phenomenon. Thereupon, equatorial region should be disregarded.

To build the winter anomaly intensity maps, we calculated the linear regressions for the midday TEC and RO N_mF_2 values in the winter and in the summer periods from the $F_{10.7A}$ index (calculated as a mean between $F_{10.7}$ and $F_{10.7m}$) in a cell.

$$\begin{aligned} \mathrm{TEC_W} &= a_W + b_W \times F_{10.7A} \\ \mathrm{TEC_S} &= a_S + b_S \times F_{10.7A} \\ \mathrm{N_mF_{2W}} &= c_W + d_W \times F_{10.7A} \\ \mathrm{N_mF_{2S}} &= c_S + d_S \times F_{10.7A} \end{aligned} \quad (1)$$

The linear regression parameters, a, b, c, d, were determined based on the least square method. Here b_W, b_S, d_W, d_S are growth rates of TEC or N_mF_2 with $F_{10.7}$ for winter (W) and summer (S), respectively. The index $F_{10.7A}$ was used by Lei et al. (2005), where it was shown that this index (in contrast to daily $F_{10.7}$) provides a linear dependence of N_mF_2 on $F_{10.7A}$. The advantage of $F_{10.7A}$ is that it takes into account both median value and short-term changes.

Based on these regressions, we calculated the winter/summer ratio (anomaly intensity) for different $F_{10.7A}$ levels in each cell.

$$\begin{aligned} TEC_W/TEC_S &= (a_W + b_W \times F_{10.7A})/(a_S + b_S \times F_{10.7A}) \\ N_mF_{2W}/N_mF_{2S} &= (c_W + d_W \times F_{10.7A})/(c_S + d_S \times F_{10.7A}) \end{aligned} \quad (2)$$

Because the GIM data set involves a large statistical interval covering different heliophysical conditions, this allowed us to analyze the winter anomaly intensity at different levels of geomagnetic activity, and to separate solar and geomagnetic effects. For that, we calculated separate sets of regression coefficient and analyzed the winter anomaly intensity both at a low level of geomagnetic activity (K_p in the last 24 h ≤ 3, by analogy with Pavlov & Pavlova (2012) and under disturbed conditions. We used two types of disturbed conditions. The first one is the current-day disturbance: K_p did not surpass 3 in the last 48 h, except recording $3 < K_p \leq 6$ at least once in the last 24 h. The second is the previous-day disturbance: K_p did not surpass 3 in the last 24 h, but, in the last 48 h, $3 < K_p \leq 6$ was recorded. Below, we use "$K_{p\text{-}1}$" for the previous day.

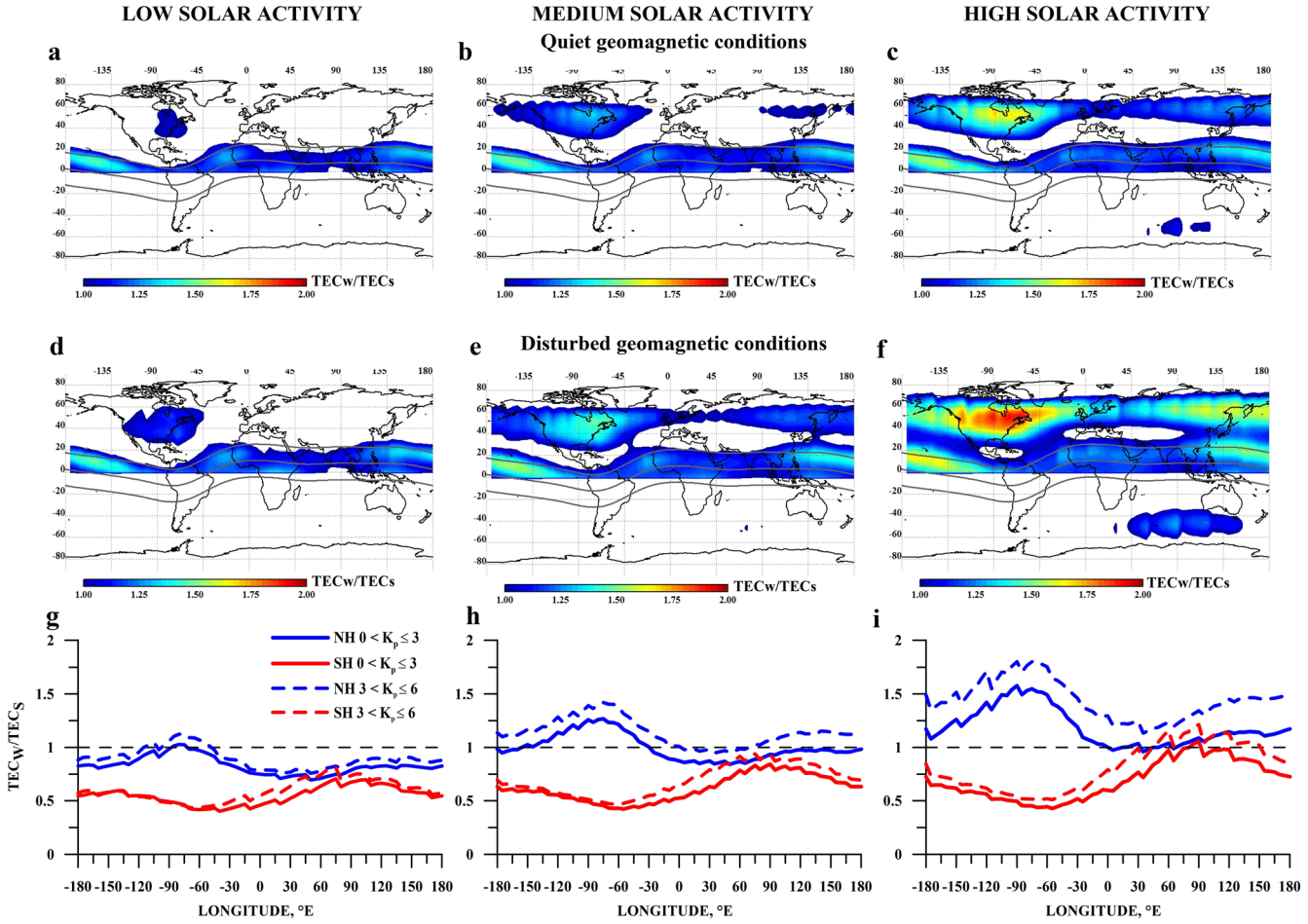

Fig. 4. Maps for the winter anomaly intensity in TEC for quiet geomagnetic conditions (a–c) and for a moderate geomagnetic disturbance ($3 < K_p \leq 6$, $K_{p\text{-}1} \leq 3$; d–f) at different levels of solar activity: −90 *s.f.u.* (a, d), −120 *s.f.u.* (b, e),−200 *s.f.u.* (c, f). Panels (g–i) show the longitudinal variations in the TEC winter anomaly intensity averaged in the 40–60° geographic latitude bands for quiet (solid lines) and disturbed (dashed lines) geomagnetic conditions. White domains on panels (a–f) correspond to the regions, for which the winter/summer ratio is less than 1. Bold gray curves (a–f) are the geomagnetic equator and ±15° geomagnetic latitudes.

Similarly, we obtained the ratios of the N_mF_2 winter values to summer ones for RO measurements. The basis of RO method was described in detail by Lee et al. (2001). When processing the COSMIC, CHAMP, and GRACE data, we split spatially the globe into cells with resolution 5° in latitude and 15° in longitude. Selected were the N_mF_2 measurements corresponding to the local midday (±1 h) time profile at the point of recording. For each cell, we accumulated the data and calculated the regression dependence on $F_{10.7A}$, by analogy to the TEC procedure described above. We failed to divide the COSMIC data into the geomagnetic activity levels due to scarce statistics; but note that the major contribution corresponds to quiet conditions.

For both TEC and N_mF_2 in each grid of mid-latitudes, there was enough data for regression analysis. The statistics is shown in Figures 1 and 2. The TEC data contain 624–676 measurements under quiet conditions ($K_p \leq 3$; Fig. 1a, b) and 122–140 measurements under disturbed conditions ($K_p \leq 3$, $3 < K_{p\text{-}1} \leq 6$; and $3 < K_p \leq 6$, $K_{p\text{-}1} \leq 3$; Fig. 1c–f). The N_mF_2 data contain ~44–95 (they are the values of the first and the third quartiles in the measurements distribution) measurements for each cell (Fig. 2).

As a result, we obtained the following data set to analyze the winter anomaly:

1) Maps for the N_mF_2 winter anomaly intensity from (Pavlov & Pavlova, 2012) for three solar activity levels. The maps are based on the data for 1957–2009.
2) Maps for the N_mF_2 winter anomaly intensity from the COSMIC, CHAMP, and GRACE data for 2001–2015 at different $F_{10.7A}$ levels.
3) Maps for the TEC winter anomaly intensity from the GIM data for 1998–2015 for different levels of solar and geomagnetic activity.

Also, we calculated the winter-to-summer ratio of TEC (see Supporting materials, Fig. S1) by using the mean values for three solar activity levels following the Pavlov & Pavlova (2012) separation method. For that purpose, we averaged all

midday TEC values in each GIM cell, when K_p does not exceed 3 for the last 24 h at the corresponding solar activity. The advantage of the linear regression approach (as compared with the averaging approach) is that this method allows us to obtain the winter-to-summer ratio at any solar activity level. It can be used to reveal the solar activity level, at which the winter anomaly phenomenon starts to be observable in different sectors of the globe, as well as the regions, where the winter anomaly phenomenon may be observed in principle.

The winter anomaly phenomenon and its longitudinal variations are accepted to be explained, basically, by neutral composition variations at thermospheric heights. The most important neutral composition parameter for the electron density distribution at F2 region heights is the O/N_2 ratio (Rishbeth & Garriott, 1969). Therefore, we analyzed the features of the O/N_2 ratio for solstice periods based on the Global Ultra-Violet Imager (GUVI) data. GUVI is a spatial scanning far-ultraviolet spectrograph operated onboard the TIMED (Thermosphere, Ionosphere, Mesosphere Energetics and Dynamics) spacecraft, launched in 2001 (Strickland et al., 2004). GUVI measures atomic oxygen 135.6 nm and the molecular nitrogen Lyman-Birge-Hopfield (LBH) dayglow emission intensity in the far ultraviolet and obtains the O/N_2 density profiles. As a product, GUVI provides daytime high-integrated O/N_2 ratio from a reference altitude up to satellite orbit. The reference altitude is determined as a height at which the height-integrated N_2 density is 10^{17} cm^{-2} (~140 km) (Christensen et al., 2003). The GUVI O/N_2 data are freely available at (http://guvitimed.jhuapl.edu/). For the analysis we used GUVI data for the period from 2002 till 2015. The GUVI data were sorted on three solar activity levels by the criteria, which were applied for obtaining averaged TEC maps (given in Supporting materials). Then, for every solar activity group, the O/N_2 values were averaged separately over the winter and summer periods in each map point and their winter/summer ratios were calculated as $(O/N_2)_W/(O/N_2)_S$, where $(O/N_2)_W$ and $(O/N_2)_S$ are the O/N_2 ratios for winter and summer conditions, accordingly.

For estimating the neutral wind influence, we used the latest Horizontal Wind Model (HWM14) updated with new observations and formulation changes (Drob et al., 2015). The resulting update provided an improved time-dependent, observationally based, global empirical specification of the upper atmospheric general circulation patterns and migrating tides. The HWM14 does not include solar activity dependence of neutral winds. For the vertical plasma transport calculations, we used the International Geomagnetic Reference Field (IGRF) model (Mandea & Macmillan, 2000).

3 Observational results

3.1 Winter anomaly in N_mF_2

Figure 3 shows the maps for the ratio of the N_mF_2 winter midday values to summer ones at three levels of solar activity: low (90 *s.f.u.*, Fig. 3a, d), medium (120 *s.f.u.*, Fig. 3b, e), and high (200 *s.f.u.*, Fig. 3c, f). The (a–c) maps were obtained based on the data from Pavlov & Pavlova (2012), the (d–f) maps were obtained from RO observations. Figure 3g–i shows variations in the N_mF_2 winter anomaly intensity averaged in the 40–60° latitude bands according to the RO data. Here and further, we used geographical coordinates. All the results are for quiet geomagnetic conditions.

One can see that the maps for the N_mF_2 anomaly intensity based on the data from individual ionosondes (a–c) and based on the regression analysis from RO observations (d–f) show good agreement. There are, however, individual local variances. For example, the ionosonde data (Fig. 3a) show the winter anomaly at low solar activity in the southern tip of South America. However, there is no winter anomaly at medium solar activity in this region. This finding is, more likely, related to different statistics.

Figure 3 shows an essential longitudinal asymmetry of the winter anomaly in N_mF_2. For the Northern Hemisphere, the winter anomaly has the greatest intensity in the North American sector. For the Southern Hemisphere, it is the Australian sector where the winter anomaly is mostly expressed, which agrees well with the theory proposed by Rishbeth (1998). The winter anomaly intensity in the East Siberian sector considerably surpasses that of the European region (Fig. 3g–i). However, according to the mechanism from (Rishbeth, 1998), the winter anomaly intensity in the East Siberian sector being the most remote from the geomagnetic pole should be minimal. The elucidation for this discrepancy requires an additional interpretation.

3.2 Winter anomaly in TEC

Figure 4a–c presents the maps for the winter anomaly intensity in TEC under quiet geomagnetic conditions ($K_p \leq 3$ in the last 24 hours). Figure 4d–f presents those under a moderate geomagnetic disturbance during the current day ($3 < K_p \leq 6$, $K_{p\text{-}1} \leq 3$). Also, we show the longitudinal variations in the TEC winter anomaly intensity averaged in the 40–60° latitude bands at different geomagnetic activity levels (g–i). Presented are the distributions of the winter anomaly intensity at three levels of the solar activity: low (90 *s.f.u.*, Fig. 4a, d, g), medium (120 *s.f.u.*, Fig. 4b, e, h), and high (200 *s.f.u.*, Fig. 4c, f, i). The maps in Figure 4 and the maps obtained by the averaging technique (Supporting materials, Fig. S1) did not reveal principal differences in spatial features.

Comparing the results presented in Figures 3 and 4, one can see that the common properties of the winter anomaly in N_mF_2 and TEC agree and are typical for different levels of solar and geomagnetic activity. The winter/summer ratio is substantially greater in the Northern Hemisphere, than that in the Southern one, both for TEC and for N_mF_2. Figures 3 and 4a–c allow comparing the winter anomaly in N_mF_2 and TEC at similar geomagnetic activity. At low solar activity, there is practically no TEC winter anomaly, except for the North American sector (Fig. 4a). Meanwhile, the N_mF_2 winter anomaly exists in all the longitudinal sectors of the Northern Hemisphere even at a low solar activity (Fig. 3d). As for N_mF_2, there is a longitudinal asymmetry of the winter anomaly in TEC for all the solar activity levels (Fig. 4g–i). The winter anomaly intensity, both for N_mF_2 and for TEC, increases with the solar activity growth.

Compared with the similar distributions under quiet geomagnetic conditions (Fig. 4a–c), the region, where the winter anomaly phenomenon is observed during moderate geomagnetic disturbances, expands, and its intensity grows (Fig. 4d–4f). In the Australian sector, the winter anomaly starts to be recordable already at 130 *s.f.u.* (see Supporting materials,

Table 1. Winter anomaly appearance in different regions.

Region	N_mF_2	TEC (Kp ≤ 3)	TEC (3 < Kp ≤ 6)
North American sector	Always	≥90 s.f.u.	≥80 s.f.u.
East Siberian sector	Always	≥120 s.f.u.	≥100 s.f.u.
Entire Northern Hemisphere	Always	≥160 s.f.u.	≥110 s.f.u.
Australian sector	≥90 s.f.u.	≥170 s.f.u.	≥130 s.f.u.

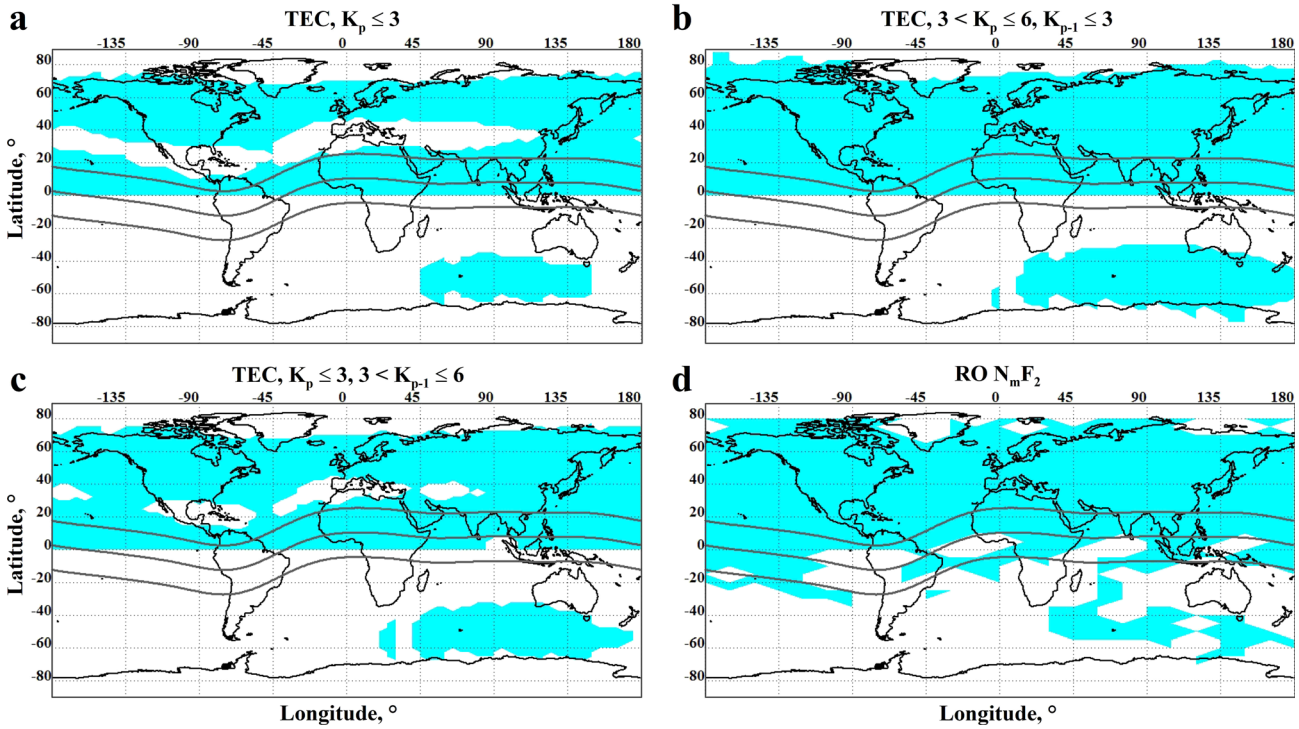

Fig. 5. Regions where one may observe the winter anomaly (blue color) in TEC (a–c) and N_mF_2 (d). (a) K_p in the last 24 h did not surpass 3; (b) K_p did not surpass 3 in the last 48 h, except recording $3 < K_p \le 6$ at least once in the last 24 h; (c) K_p in the last 24 h did not surpass 3, but in the last 48 h it was recorded $3 < K_{p-1} \le 6$. For N_mF_2 (d) there was no K_p separation. Bold gray curves are the geomagnetic equator and ±15° geomagnetic latitudes.

Fig. S4), and, at 200 *s.f.u.*, it encompasses a large longitudinal sector. However, the pattern of the winter anomaly intensity spatial distribution generally persists.

Note here, so far as geomagnetic disturbances are stochastic events which may last a few days, it may be not sufficient to examine geomagnetic conditions for only one previous day to properly consider the influence of geomagnetic disturbances. Therefore, we also carried out an analysis of the winter anomaly intensity in TEC using the data separation according to the integral $A_{p\tau}$ index (Wrenn, 1987), which allows to more correctly consider the prolonged influence of geomagnetic disturbances (Deminov et al., 2013). $A_{p\tau}$ is the mean weighed (with the 11-h characteristic time) value of the 3-h linear geomagnetic activity index *ap*. The results are given in Supporting materials (Fig. S2). One may see that the distributions of winter anomaly intensity for both methods of data separation are almost identical. Apparently, large data statistics, especially for the geomagnetically quiet period, in our case makes it possible to avoid potential errors connected with prolonged geomagnetic disturbances. Therefore, we show here the results that were obtained for the data separation according to K_p values, since this is a widely-used index.

Using the regression procedure allowed us to reveal the solar activity levels, at which the winter anomaly starts to be recordable in different geographical sectors. For this purpose, we considered the maps of winter anomaly in TEC obtained for $F_{10.7A}$ levels from 70 till 270 at 10 *s.f.u.* spacing. Then for each locations of the globe we fixed the lowest $F_{10.7A}$ value, at which the winter anomaly phenomenon ($TEC_W/TEC_S > 1$) appears according to observation data. The same was done for N_mF_2 maps. All these maps are given in Supporting materials (Figs. S1–S6). Table 1 summarizes the results. The accuracy of the obtained values is 10 *s.f.u.*

3.3 Where may the winter anomaly be observed?

Accounting for the experimental findings that the region, where the winter anomaly occurs, expands with the solar activity increase, one may assume that, at a certain level of solar activity, it will be possible to observe the winter anomaly

worldwide. In reality, this does not prove to be true. We tried to answer the question: "And where may one ever record the winter anomaly?"

For this purpose, one should compare the growth rates of TEC or N_mF_2 with $F_{10.7A}$ from Expression (1) for winter (b_W or d_W) and summer (b_S or d_S). For each map point, we consider that, as long as $b_W > b_S$ or $d_W > d_S$, then, in the first approximation, there is a principal possibility to observe the winter anomaly in this point at least for some level of solar activity.

Figure 5 shows the regions (blue colors), where the winter anomaly may be observed in TEC (a–c) and in N_mF_2 (d). We analyzed a possibility to observe the TEC winter anomaly for different levels of geomagnetic activity. Figure 5a presents the results corresponding to quiet geomagnetic conditions ($K_p \leq 3$ in the last 24 h); Figure 5b is for moderately disturbed conditions during current day ($3 < K_p \leq 6$, $K_{p\text{-}1} \leq 3$); Figure 5c presents the results corresponding to the disturbance on the previous day, when K_p did not surpass 3 in the last 24 h, but in the last 48 h, $3 < K_{p\text{-}1} \leq 6$ ($K_p \leq 3$, $3 < K_{p\text{-}1} \leq 6$) was recorded. Figure 5d shows a possibility to observe the N_mF_2 winter anomaly integrally for all the levels of geomagnetic activity.

There is a white domain in the 20–40°N latitudes of European-African sector (Fig. 4b, c, e, f). It is clear especially under disturbed geomagnetic conditions. In this region, the effect of the solar zenith angle (direct ionization) exceeds the joint effect of the winter anomaly formation mechanisms. The region decreases with the solar activity growth.

One can see that, at mid-latitudes of the Northern Hemisphere, the winter anomaly, both in TEC and in N_mF_2, may be observed everywhere. At the moderately-disturbed geomagnetic activity (Fig. 5b), the winter anomaly may be recorded practically in all the Northern Hemisphere.

In the Australian region, the winter anomaly domain under quiet geomagnetic conditions occupies the 45°–150°E longitude range and the −65°N through −35°N latitude range. At the geomagnetic activity growth, the domain, where the TEC winter anomaly may be recorded, considerably expands. Moreover, even if over the last day the geomagnetic conditions were quiet, but a moderate magnetic disturbance was recorded the day before ($3 < K_{p\text{-}1} \leq 6$), the domain, where the winter anomaly may be observed, also expands (Fig. 5c). We note, however, that according to Figure 5, in the Southern Hemisphere, under any geophysical conditions, the winter anomaly may not be observed anywhere, except for the Australian sector.

The N_mF_2 winter anomaly may be observed in the same regions, as the TEC winter anomaly (Fig. 5d). In the Northern Hemisphere, the N_mF_2 winter anomaly may occur everywhere, whereas in the Southern Hemisphere, it may be recordable only in the Australian region.

4 Discussion

The analysis allowed us to corroborate the known properties of the winter anomaly and to reveal a number of new peculiarities. Among the earlier known regularities, we note the following:

(a) Regardless of the geographic position, the winter anomaly intensity increases with the solar activity growth. This feature results from the fact that $O^+ + N_2$ reaction rate coefficient, and, as a result, N_mF_2, depend on solar activity growth in winter and summer differently (Mikhailov & Perrone, 2011). Additionally, Burns et al. (2015) showed that vertical winds act stronger on O/N_2 gradients at solar maximum than they do at solar minimum, (and as a result stronger winter-to-summer difference of O/N_2 occurs) due to different vertical temperature gradients between 100 and 200 km at solar maximum and minimum.

(b) The winter anomaly intensity is essentially greater in the Northern Hemisphere than that in the Southern one. This peculiarity in the spatial distribution of the winter anomaly may be partly elucidated through the effect of the interhemispheric asymmetry (annual anomaly). The effect is that the ionosphere electron density in the Northern and Southern Hemispheres in December is always essentially higher, than that in June practically everywhere (Mendillo et al., 2005). It is difficult to separate the formation mechanisms (as well as the morphology) of the winter anomaly from those for the annual anomaly.

(c) The greatest winter/summer ratio is observed in the North American sector for the Northern Hemisphere and in the Australian sector for the Southern one, which agrees with the theory proposed by Rishbeth (1998).

We refer the following peculiarities to those unnoted earlier as new knowledge on the issue of winter anomaly:

(a) One of important finding of this study is that the least value of the winter anomaly intensity for the Northern Hemisphere is observed in the East European sector. To a certain degree, this feature can be found in previous studies. The Torr & Torr (1973) maps indicated that the f_oF_2 winter-summer difference in the Northern Hemisphere was the least over Europe under high solar activity, but this was not the subject of discussion in the Torr & Torr (1973) paper. Using TEC values from GPS stations during 2002, Huo et al. (2009) concluded that the TEC winter anomaly is stronger in the Russia-Asia region than in Europe due to corresponding changes in the O/N_2 ratio. Longitudinal variation in the daytime winter anomaly indicator obtained from the COSMIC N_mF_2 measured in 2007 (Lee et al., 2011) demonstrated that this indicator was the least at longitudes of 0–60 °E. Lee et al. (2011) did not discuss this minimum and concluded that their results were consistent with the Rishbeth (1998) explanation (although it was not true). Our paper generalizes the previous studies and for the first time shows that the stronger winter anomaly in the Asian sector than that in the European one is a universal feature observed both in TEC and N_mF_2 at all the levels of solar and geomagnetic activities. The importance of this finding lies in the fact that does not agree with the theory proposed by Rishbeth (1998) and the confirmation of this theory by the CTIP model calculations (Zou et al., 2000). Thus, the explanation of the longitudinal variation of winter anomaly most commonly accepted today (Rishbeth, 1998; Rishbeth et al., 2000; Zou et al.,

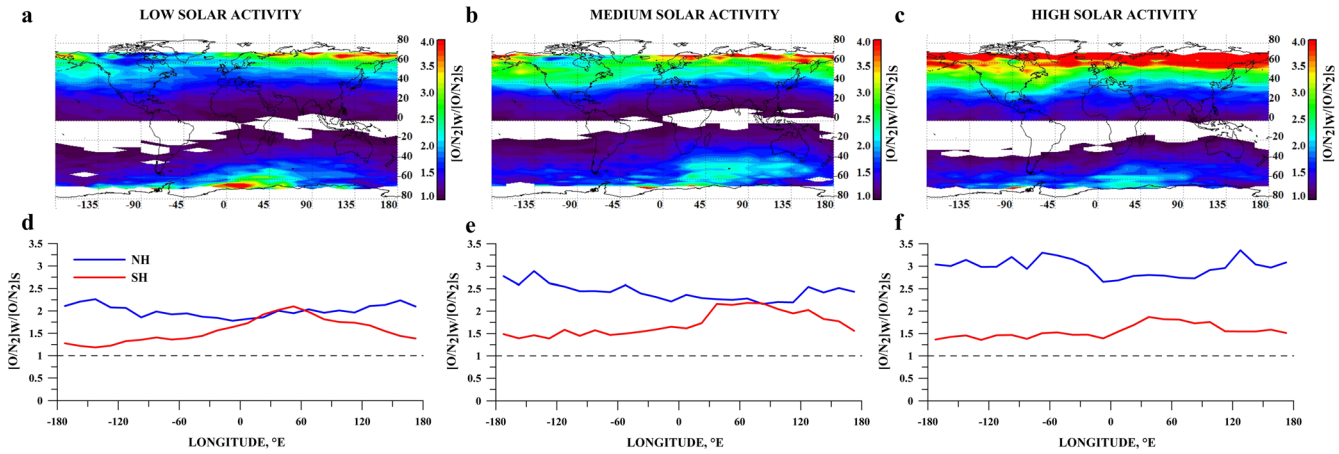

Fig. 6. Maps for the winter anomaly intensity in O/N_2 ratio at different levels of solar activity (a)–(c). White domains correspond to the regions, for which the winter/summer ratio is less than 1. Panels (d)–(f) show the longitudinal variations of the winter anomaly intensity in the O/N_2 ratio, averaged in the 40–60° geographic latitude bands in the Northern (blue) and Southern (red) Hemispheres.

2000) needs modifying and/or supplementing. There has been no theory to explain the winter anomaly longitudinal variation so far, except the Rishbeth theory. All the papers devoted to longitudinal variation of the winter anomaly are based on the Rishbeth theory (Mendillo et al., 2005; Lee et al., 2011). Therefore, it is very important to highlight this problem.

(b) A geomagnetic disturbance growth facilitates the winter anomaly intensity increase. This effect may be elucidated through the peculiarities of the ionosphere response to geomagnetic disturbances in winter and summer periods. It is known (Buonsanto, 1999) that, magnetic storms predominantly lead to the electron density negative response in summer and to a positive one in winter at mid-latitudes. As a result, the winter/summer ratio during a disturbed period increases. We also note that the geomagnetic disturbances affect the winter anomaly intensity, even if these disturbances occur within 24–48 h prior to observations.

(c) We determined, for the first time, the values of the solar activity level, at which the winter anomaly phenomenon starts to be observable in different sectors of the globe. Under quiet geomagnetic conditions, the winter anomaly in TEC appears at 90 *s.f.u.* in the North American region, at 120 *s.f.u.* – in the East Siberian region, at 160 *s.f.u.* – at all middle latitudes of the Northern Hemisphere, and at 170 *s.f.u.* – in the Australian region. For moderate disturbances, those values are 80, 100, 110, and 130 *s.f.u.*, respectively. For N_mF_2, in the Northern Hemisphere, the winter anomaly is a characteristic phenomenon, and is observed even at lower thresholds for the solar radiation level. In the Southern Hemisphere, the N_mF_2 winter anomaly starts to be observable at 90 *s.f.u.*

(d) We also revealed the regions, where the winter anomaly phenomenon may be observed in principle. At mid-latitudes of the Northern Hemisphere, the winter anomaly phenomenon may be recorded almost everywhere, whereas, in the Southern Hemisphere, at any level of solar activity, the winter anomaly may be observed only in the revealed domain of the Australian sector. With the geomagnetic activity increase, this domain expands. We should note that, at mid-latitudes of the Northern Hemisphere under quiet geomagnetic conditions, there is a region (~20–40°N), where there is no winter anomaly. The region decreases with solar activity increase.

(e) Based on the comparison between the winter anomaly peculiarities in N_mF_2 and TEC, we show that the winter anomaly fundamental features (spatial distribution and solar activity dependence) are similar for these parameters. However, the TEC winter anomaly evolves significantly weaker, than that in N_mF_2. This fact is elucidated by the essential difference between the half-thicknesses of the electron density winter and summer profiles. According to (Mikhailov & Perrone, 2014), the small half-thickness of the electron density winter profile, $N_e(h)$, as compared with that of the summer one, is the reason for the winter/summer ratio decrease at the heights different from the maximal ones.

The winter anomaly phenomenon and its longitudinal variations are abovementioned to be explained, basically, by the neutral composition at thermospheric heights, and especially by the O/N_2 ratio distribution. Figure 6a–c shows maps of $(O/N_2)_W/(O/N_2)_S$, obtained from GUVI data, and Figure 6d–f shows longitudinal variations in $(O/N_2)_W/(O/N_2)_S$ over the 40–60° latitude bands in the Northern and Southern Hemispheres for the three solar activity levels. One can see that the pattern of winter anomaly in ionospheric parameters (N_mF_2, TEC) and O/N_2 ratio are in a good agreement in general, with the exception of individual details. In particular, the distributions of the O/N_2 winter-to-summer ratio can explain the following features of the ionospheric winter anomaly: (1) significant excess of the winter anomaly intensity in the Northern Hemisphere over the Southern one at any solar activity level; (2) enhancement in the winter anomaly intensity with increasing solar activity level; and (3) longitudinal variations in the winter anomaly intensity in the Southern Hemisphere with a maximum in the Australian sector.

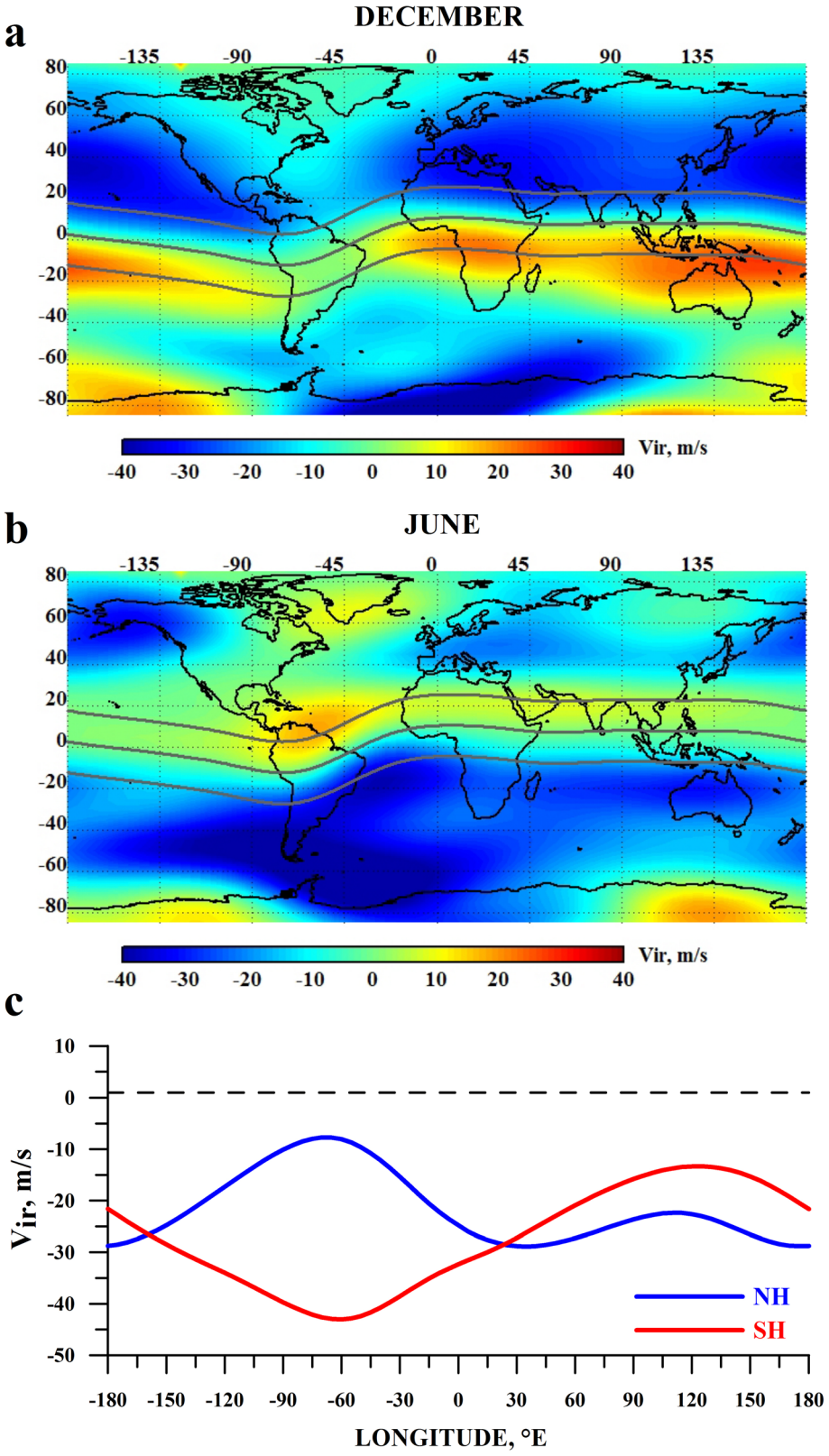

Fig. 7. Maps for the daytime vertical plasma transport caused by horizontal thermospheric wind at December and June solstice (a), (b). Panel (c) shows the local winters longitudinal variations of the vertical plasma transport averaged in the 40–60° geographic latitude bands in the Northern (blue) and Southern (red) Hemispheres. Bold gray curves (a), (b) are the geomagnetic equator and ±15° geomagnetic latitudes.

Table 2. N_mF_2 (North, Dec), N_mF_2 (North, Jun), N_mF_2 (South, Dec), and N_mF_2 (South, Jun) calculated from the RO observations, as well as R_N, R_S, R_D, and R_J ratios.

$F_{10.7A}$ (sfu)	N_mF_2 (North, Dec)	N_mF_2 (North, Jun)	N_mF_2 (South, Dec)	N_mF_2 (South, Jun)	R_N	R_S	R_D	R_J
70	3.61	3.06	3.78	2.63	1.18	0.69	0.96	0.86
140	9.64	5.91	8.49	6.33	1.63	0.75	1.14	1.07
200	17.14	9.11	14.04	10.82	1.88	0.77	1.22	1.19

However, it is important to note that there are features which cannot be attributed to O/N_2 behavior. The strongest discrepancy between the winter anomaly intensity in O/N_2 and ionospheric electron density is revealed for the longitudinal variations in the Northern Hemisphere. At all solar activity levels, there is a distinct maximum of the winter anomaly intensity in TEC and N_mF_2 in the North American sector and a minimum in the European one. While the greatest winter anomaly intensity in O/N_2 at middle latitudes is seen in the Far Eastern region at low and medium solar activity. Thus, the explanation of longitudinal variations in ionospheric winter anomaly for the Northern Hemisphere requires consideration of additional mechanisms.

As such an additional driver of longitudinal variations in the intensity of the winter anomaly in TEC and N_mF_2, we consider the vertical plasma transport caused by zonal electric field and horizontal thermospheric wind (Rishbeth, 1972). Based on a preliminary analysis of the $E \times B$ drift velocity measurements, obtained with the midlatitude incoherent scatter radars (Richmond, 1976; Richmond et al., 1980), it can be concluded that the vertical velocity of daytime $E \times B$ plasma drift is insignificant. Although this issue remains open due to the lack of a global network of incoherent scatter radar measurements. Therefore, in the study, to analyze the longitudinal variations, we neglected the electric field effects and used only daytime thermospheric wind velocities for vertical plasma transport estimation. The velocities were obtained from the HWM14 empirical model (Drob et al., 2015). In the spherical geographical coordinate system, the daytime vertical plasma velocity, V_{ir}, related to the drag effect with horizontal neutral wind can be expressed as the following: $V_{ir} = (V_{n\theta} \cos D + V_{n\lambda} \sin D) \sin I \cos I$, where $V_{n\theta}$ and $V_{n\lambda}$ are the meridional (positive southward) and zonal (positive eastward) components of the thermospheric wind velocity, respectively, D and I are the geomagnetic declination and inclination, respectively, obtained from the IGRF model (Mandea & Macmillan, 2000).

The obtained maps of daytime vertical plasma transport for the December and June solstice are presented in Figure 7a, b. The negative vertical velocity leads to the plasma transport to lower heights with higher recombination rate, which in turn results in the F2-region electron density reduction (Rishbeth & Garriott, 1969). As seen from Figure 7a, b, the daytime vertical velocity is mainly negative, and thus, the smaller modulus of negative velocity, the higher N_mF_2 and TEC are expected. The longitudinal variations in the vertical plasma transport for local winters in the Northern and Southern Hemispheres (Fig. 7c) reveal the following features: (1) for the Northern Hemisphere the smallest modulus of negative velocity is seen in the North American sector and the largest one in the East European sector; (2) for the Southern Hemisphere the smallest velocity modulus is seen in the Australian sector and the largest one in the South American sector; (3) on average the modulus of negative velocity is larger in the Southern Hemisphere than in the Northern one. The feature (1) explains the longitudinal variations in ionospheric winter anomaly for the Northern Hemisphere, which cannot be completely explained by O/N_2 behavior. The feature (2) enhances O/N_2 impact on the longitudinal variations in ionospheric winter anomaly for the Southern Hemisphere. The feature (3) enhances the interhemispheric asymmetry of the winter anomaly intensity in TEC and N_mF_2. Note that the efficiency of the vertical plasma transport impact on TEC and N_mF_2 is noticeably higher in local winter than in local summer (Prölss, 1995; Mikhailov, 2000), and therefore we do not consider vertical transport effects in local summer.

In our opinion, there is both solar (determined by geographical latitude) and geomagnetic control (determined by geomagnetic latitude) of the winter anomaly intensity. Thus, neither geographic nor geomagnetic latitudes are invariant for the longitude variations of the winter anomaly intensity. So, using the corrected geomagnetic coordinates,[1] we have obtained the global plots of the winter anomaly intensity in geomagnetic latitude – geographic longitude coordinate system. The figure for TEC is presented in the Supporting Information (SI, Fig. S7). As seen from the figure, the contours of winter anomaly intensity and the white area, corresponding to the anomaly absence, at lower mid-latitudes are straighten compared to the maps in geographical coordinates. At the same time, contours at higher latitudes are distinctly curved: the intensity maxima are seen at geomagnetic latitude ~60° MLat in the in the American sector and at ~50° MLat in the East Siberian sector. From this we can make a preliminary conclusion that the geomagnetic control of the winter anomaly prevails at lower mid-latitudes, while at higher mid-latitudes the geomagnetic control weakens and the solar control influence increases.

Finally, we compared the features of the winter anomaly by different definitions. Burns et al. (2012, 2014) proposed an alternative definition of the winter anomaly as the ratio of N_mF_2 in the winter hemisphere to N_mF_2 in the summer hemisphere for the same day (December or June soltice). For this purpose, we calculated RO N_mF_2 averaged throughout 40–60° latitude bands and all longitudes for December and June in the Northern Hemisphere (N_mF_2(North, Dec) and N_mF_2(North, Jun), respectively) and did the same for the Southern Hemisphere (N_mF_2(South, Dec) and N_mF_2(South, Jun), respectively). In accordance with historical definition (Berkner et al., 1936), the winter anomaly is calculated by the ratios:

[1] Tsyganenko N.A. GEOPACK. 2008. A set of Fortran subroutines for computations of the geomagnetic field in the Earth's magnetosphere, 2008, http://geo.phys.spbu.ru/~tsyganenko/modeling.html. Access date: 19 September 2018.

$$R_N = \mathrm{N_mF_2(North, Dec)/N_mF_2(North, Jun)}$$

$$\text{and} \quad R_S = \mathrm{N_mF_2(South, Jun)/N_mF_2(South, Dec)}$$

for the Northern and Southern Hemisphere, respectively. Whereas in accordance with the definition of Burns et al. (2012, 2014), the winter anomaly is calculated by the ratios:

$$R_D = \mathrm{N_mF_2(North, Dec)/N_mF_2(South, Dec)}$$

$$\text{and} \quad R_J = \mathrm{N_mF_2(South, Jun)/N_mF_2(North, Jun)}$$

for the December or June solstice, respectively. Table 2 presents calculated R_N, R_S, R_D, and R_J ratios for three solar activity levels. One may see that:

$$\mathrm{N_mF_2(South, Dec)} > \mathrm{N_mF_2(North, Dec)} > \mathrm{N_mF_2(North, Jun)} > \mathrm{N_mF_2(South, Jun)}$$

at low solar activity, and

$$\mathrm{N_mF_2(North, Dec)} > \mathrm{N_mF_2(South, Dec)} > \mathrm{N_mF_2(South, Jun)} > \mathrm{N_mF_2(North, Jun)}$$

at moderate and high solar activity.

These N_mF_2 relationships lead the following features of the winter anomaly ratios:

1. $R_N > 1$ at any solar activity level;
2. $R_S < 1$ at any solar activity level;
3. R_D and $R_J < 1$ at low solar activity, and R_D and $R_J > 1$ at moderate and high solar activity.

Feature (3) is in complete agreement with the Burns et al. (2014) conclusion that the winter anomaly does not appear when the $F_{10.7}$ is below a value of about 90–100 *s.f.u.* but exists under higher solar activity. It contradicts with features of winter anomaly under the historical definition. We do not undertake to state which of the definitions is more correct, but we emphasize that different definitions lead to different features of the winter anomaly.

5 Conclusion

Based on the comparison between the winter anomaly peculiarities in N_mF_2 and in TEC, we showed that the winter anomaly fundamental features (spatial distribution and solar activity dependence) are similar for these parameters.

Our paper generalizes the previous studies and, for the first time, shows that the stronger winter anomaly in the Asian sector than that in the European one is a universal feature observed both in TEC and N_mF_2 at all the levels of solar and geomagnetic activities.

For the first time we found that a geomagnetic disturbance growth facilitates the winter anomaly intensity increase.

We determined the values of the solar activity level, at which the winter anomaly phenomenon starts to be observable in different sectors of the globe and revealed the regions, where the winter anomaly phenomenon may be observed in principle.

We consider the obtained results in the context of spatial and solar cycle variations in the O/N_2 ratio and vertical plasma transport caused by meridional thermospheric wind. We conclude that many features of the ionospheric winter anomaly can be explained by O/N_2 behavior. At the same time, the longitudinal variations in the ionospheric winter anomaly for the Northern Hemisphere (including a disagreement with the Rishbeth theory) may be related to the longitudinal variations of the vertical plasma transport induced by thermospheric wind in local winter.

Additionally, we discussed the winter anomaly by different definitions and showed that different definitions lead to different features of the winter anomaly. For the latitude-longitude averaged N_mF_2, the winter anomaly, by its historical definition, exists in the Northern Hemisphere and is absent in the Southern one at any solar activity level. The winter anomaly, by the Burns' et al. (2012, 2014) definition, is absent at low solar activity and is present at moderate and high solar activity.

We hope that the results of our investigations facilitate developing the Rishbeth theory with regard to longitudinal variability of the winter anomaly, and stimulate a fruitful discussion of ionospheric interhemispheric asymmetry (annual anomaly).

Acknowledgements. We are grateful to the Reviewers for their valuable comments. We express our gratitude to the Jet Propulsion Laboratory and NASA's Archive of Space Geodesy Data for the Global Ionospheric Maps data (ftp://cddis.gsfc.nasa.gov/gps/products/ionex); to the GFZ and UCAR teams for making CHAMP, GRACE (GFZ) and COSMIC (UCAR) radio occultation data available (http://cdaac-www.cosmic.ucar.edu/cdaac/products.html); as well as to NOAA's National Centers for Environmental Information for helio-geomagnetic indexes data (http://www.ngdc.noaa.gov/stp/GEOMAG/ kp_ap.html). We express our gratitude to the IGRF (http://www.geomag.bgs.ac.uk/ data_service/models_compass/igrf.html) and HWM14 model's teams. The GUVI data (http://guvitimed.jhuapl.edu/) used in the study are provided through support from the NASA MO&DA program. The GUVI instrument was designed and built by the Aerospace Corporation and the Johns Hopkins University (A.B. Christensen, L.J. Paxton). Also, we are thankful to A.V. Pavlov and N.M. Pavlova, whose results were used in our study. We thank Yu. M. Kaplunenko for language assistance. Analysis of the winter anomaly through GPS data were performed under the Russian Science Foundation Grant No. 17-77-20005 (Yu. Yasyukevich). The Russian Foundation for Basic Research supported analysis of radio occultation data and neutral atmosphere wind model (Grant No. 18-55-52006; K. Ratovsky, M. Klimenko, V. Klimenko; N. Chirik), as well as studying the neutral atmosphere effects (Grant No. 16-35-60018; A. Yasyukevich). In the study we used the algorithms obtained within the budgetary funding of Basic Research program II.16. The editor thanks Matthias Förster and Estefania Blanch for their assistance in evaluating this paper.

Supplementary Material

The supporting material (Figs. S1 to S6) is available at https://swsc.org/10.1051/swsc/2018036/olm

References

Afraimovich EL, Astafyeva EI, Zhivetiev IV, Oinats AV, Yasyukevich Yu V. 2008. Global electron content during solar cycle 23. *Geomagn Aeron* **48(2)**: 187–200. DOI: 10.1007/s11478-008-2008-1.

Berkner LV, Wells HW, Seaton SF. 1936. Characteristics of the upper region of the ionosphere. *Terr Magn Atmos Electr* **41(2)**: 173–184. DOI: 10.1029/TE041i002p00173.

Boenkova NM, Mednikova NV. 1972. The seasonal anomaly at the latitudes below the electron concentration maximum of F2-layer depending on latitude and time. *Geomagn Aeron* **12**: 335–337 (in Russian).

Buonsanto MJ. 1999. Ionospheric storms: A review. *Space Sci Rev* **88(3–4)**: 563–601. DOI: 10.1023/A:1005107532631.

Burns AG, Solomon SC, Wang W, Qian L, Zhang Y, Paxton LJ. 2012. Daytime climatology of ionospheric N_mF_2 and hmF2 from COSMIC data *J Geophys Res* **117**: A09315. DOI: 10.1029/2012JA017529.

Burns AG, Wang W, Qian L, Solomon SC, Zhang Y, Paxton LJ, Yue X. 2014. On the solar cycle variation of the winter anomaly. *J Geophys Res (Space Phys)* **119**: 4938–4949. DOI: 10.1002/2013JA019552.

Burns AG, Solomon SC, Wang W, Qian L, Zhang Y, Paxton LJ, Yue X, Thayer JP, Liu HL. 2015. Explaining solar cycle effects on composition as it relates to the winter anomaly. *J Geophys Res (Space Phys)* **120(7)**: 5890–5898. DOI: 10.1002/2015JA021220.

Christensen AB, Paxton LJ, Avery S, Craven J, Crowley G, et al. 2003. Initial observations with the Global Ultraviolet Imager (GUVI) in the NASA TIMED satellite mission. *J Geophys Res* **108**: 1451. DOI: 10.1029/2003JA009918.

Deminov MG, Deminova GF, Zherebtsov GA, Polekh NM. 2013. Statistical properties of variability of the quiet ionosphere F2-layer maximum parameters over Irkutsk under low solar activity. *Adv Space Res* **51**: 702–711. DOI: 10.1016/j.asr.2012.09.037.

Drob DP, Emmert JT, Meriwether JW, Makela JJ, Doornbos E, et al. 2015. An update to the Horizontal Wind Model (HWM): The quiet time thermosphere. *Earth Space Sci* **2**: 301–319. DOI: 10.1002/2014EA000089.

Fatkullin MN. 1970. The seasonal anomaly in the electron density of the topside F2-region. *J. Atm. Terr. Phys.* **32**: 1067–1075. DOI: 10.1016/0021-9169(70)90118-2.

Hernández-Pajares M, Juan JM, Sanz J, Orus R, Garcia-Rigo A, Feltens J, Komjathy A, Schaer SC, Krankowski A. 2009. The IGS VTEC maps: a reliable source of ionospheric information since 1998. *J Geodesy* **83(3–4)**: 263–275. DOI: 10.1007/s00190-008-0266-1.

Huo XL, Yuan YB, Ou JK, Zhang KF, Bailey GJ. 2009. Monitoring the global-scale winter anomaly of total electron contents using GPS data. *Earth Planet Space* **61**: 1019–1024. DOI: 10.1186/BF03352952.

King JW, Hawkins GL, Seabrook C. 1968. The seasonal behaviour of the topside, ionosphere. *J. Atm. Terr. Phys.* **30(9)**: 1701–1706. DOI: 10.1016/0021-9169(68)90018-4.

Lee LC, Rocken C, Kursinski ER. 2001. Applications of constellation observing system for meteorology, ionosphere, and climate, Springer-Verlag, Hong Kong, ISBN-10: 9789624301359 / ISBN-13: 978–9624301359

Lee WK, Kil H, Kwak Y-S, Wu Q, Cho S, Park JU. 2011. The winter anomaly in the middle-latitude F region during the solar minimum period observed by the Constellation Observing System for Meteorology, Ionosphere, and Climate. *J Geophys Res* **116**: A02302. DOI: 10.1029/2010JA015815.

Lee WK, Kil H, Kwak Y-S, Wu Q. 2014. Reply to comment by A.V. Mikhailov and L. Perrone on "The winter anomaly in the middle-latitude F region during the solar minimum period observed by the Constellation Observing System for Meteorology, Ionosphere, and Climate". *Physics* **119**: 7979–7980. DOI: 10.1002/2014JA020445.

Lei J, Liu L, Wan W, Zhang S-R. 2005. Variations of electron density based on long-term incoherent scatter radar and ionosonde measurements over Millstone Hill. *Radio Sci* **40**: RS2008, DOI: 10.1029/2004RS003106

Mandea M, Macmillan S. 2000. International Geomagnetic Reference Field – the eighth generation. *Earth Planet Space* **12**: 1119–1124. DOI: 10.1186/BF03352342

Mannucci AJ, Wilson BD, Yuan DN, Ho CH, Lindqwister UJ, Runge TF. 1998. A global mapping technique for GPS-derived ionospheric TEC measurements. *Radio Sci* **33**: 565–582. DOI: 10.1029/97RS02707.

Mendillo M, Huang CL, Pi X, Rishbeth H, Meier R. 2005. The global ionospheric asymmetry in total electron content. *J Atm Solar-Terr Phys* **67**: 1377–1387. DOI: 10.1016/j.jastp.2005.06.021.

Mikhailov AV. 2000. Ionospheric F2-layer storms. *Física de la Tierra* **12**: 223–262.

Mikhailov AV, Perrone L. 2011. On the mechanism of seasonal and solar cycle N_mF_2 variations: A quantitative estimate of the main parameters contribution using incoherent scatter radar observations. *J. Geophys. Res.* **116**: A03319. DOI: 10.1029/2010JA016122

Mikhailov AV, Perrone L. 2014. Comment on "The winter anomaly in the middle-latitude F region during the solar minimum period observed by the Constellation Observing System for Meteorology, Ionosphere, and Climate" by W. K. Lee, H. Kil, Y.-S. Kwak, Q. Wu, S. Cho, and J. U. Park. *J Geophys Res (Space Phys)* **119**: 7972–7978. DOI: 10.1002/2014JA020185

Pavlov AV, Pavlova NM. 2005. Causes of mid-latitude N_mF_2 winter anomaly at solar maximum. *J Atm Solar-Terr Phys* **67**: 862–877. DOI: 10.1016/j.jastp.2005.02.009.

Pavlov AV, Pavlova NM. 2012. Variations in statistical parameters of the N_mF_2 winter anomaly with latitude and solar activity. *Geomagn. Aeron.* **52**: 335–343. DOI: 10.1134/S0016793212030127.

Prölss GW. 1995. Ionospheric F-region storms. In: *Handbook of atmospheric electrodynamics*, H Volland (Ed.),**2**, CRC Press, Boca Raton, FL, 195–248

Qian L, Burns AG, Wang W, Solomon SC, Zhang Y, Hsu V. 2016a. Effects of the equatorial ionosphere anomaly on the interhemispheric circulation in the thermosphere. *J Geophys Res (Space Phys)*, **121**, 2522–2530. DOI: 10.1002/2015JA022169.

Qian L, Burns AG, Wang W, Solomon SC, Zhang Y. 2016b. Longitudinal variations of thermospheric composition at the solstices. *J Geophys Res (Space Phys)* **121**: 6818–6829. DOI: 10.1002/2016JA022898.

Richmond AD, Blanc M, Emery BA, Wand RH, Fejer BG, Woodman RF, Ganguly S, Amaenc P, Behnke RA, Calderon C, Evans JV. 1980. An empirical model of the quiet-day ionospheric electric fields at middle and low latitudes. *J Geophys Res* **85**: 4658–4664. DOI: 10.1029/JA085iA09p04658.

Richmond AD. 1976. Electric fields in the ionosphere and plasmasphere on quiet days. *J Geophys Res* **81**: 1447–1450. DOI: 10.1029/JA081i007p01447.

Rishbeth H. 1972. Thermospheric winds and the F-region: A review. *J Atm Terr Phys* **34**: 1–47. DOI: 10.1016/0021-9169(72)90003-7.

Rishbeth H. 1998. How the thermospheric circulation affects the ionosphere. *J Atm Sol-Terr Phys* **60**: 1385–1402. DOI: 10.1016/S1364-6826(98)00062-5.

Rishbeth H, Garriott OK. 1969. *Introduction to Ionospheric Physics*. Academic Press: New York.

Rishbeth H, Muller-Wodarg ICF, Zou L, Fuller-Rowell TJ, Millward GH, Moffett RJ, Idenden DW, Aylward AD. 2000. Annual and semiannual variations in the ionospheric F2-layer: II: physical discussion. *Ann Geophys* **18**: 945–956. DOI: 10.1007/s00585-000-0945-6.

Strickland DJ, Meier RR, Walterscheid RL, Craven JD, Christensen AB, Paxton LJ, Morrison D, Crowley G. 2004. Quiet-time seasonal behavior of the thermosphere seen in the far ultraviolet dayglow. *J. Geophys. Res.* **109**: A01302. DOI: 10.1029/2003JA010220.

Torr DG, Torr MR, Richards PG. 1980. Causes of the F region winter anomaly. *Geophys Res Lett* **7**: 301–304. DOI: 10.1029/GL007i005p00301.

Torr MR, Torr DG. 1973. The seasonal behaviour of the F2-layer of the ionosphere. *J Atm Terr Phys* **35**: 2237–2251. DOI: 10.1016/0021-9169(73)90140-2.

Wrenn GL. 1987. Time-weighted accumulations ap(τ) and Kp(τ). *J Geophys Res* **92**: 10125–10129. DOI: 10.1029/JA092iA09p10125.

Zhao B, Wan W, Liu L, Mao T, Ren Z, Wang M, Christensen AB. 2007. Features of annual and semiannual variations derived from the global ionospheric maps of total electron content. *Ann Geophys* **25**: 2513–2527. DOI: 10.5194/angeo-25-2513-2007.

Zou L, Rishbeth H, Müller-Wodarg ICF, Aylward AD, Millward GH, Fuller-Rowell TJ, Idenden DW, Moffett RJ. 2000. Annual and semiannual variations in the ionospheric F2-layer. I. Modelling. *Ann Geophys* **18**: 927–944. DOI: 10.1007/s00585-000-0927-8.

Cite this article as: Yasyukevich Y, Yasyukevich A, Ratovsky K, Klimenko M, Klimenko V, et al. 2018. Winter anomaly in N_mF_2 and TEC: when and where it can occur. *J. Space Weather Space Clim.* **8**, A45.